remote sensing

MDPI

Article

Temperature Is a Key Factor Affecting Total Phosphorus and Total Nitrogen Concentrations in Northeastern Lakes Based on Sentinel-2 Images and Machine Learning Methods

Haoming Qin [1], Chong Fang [2,*], Ge Liu [3], Kaishan Song [3,4], Zhuoshi Li [1,5], Sijia Li [3], Hui Tao [3] and Zhaojiang Yan [6]

[1] College of Computer Science and Technology, Jilin Agricultural University, Changchun 130118, China
[2] State Key Laboratory of Black Soils Conservation and Utilization, Northeast Institute of Geography and Agroecology, Chinese Academy of Sciences, Changchun 130102, China
[3] Northeast Institute of Geography and Agroecology, Chinese Academy of Sciences, Changchun 130102, China
[4] School of Geography and Environment, Liaocheng University, Liaocheng 252059, China
[5] College of Plant Protection, Jilin Agricultural University, Changchun 130118, China
[6] School of Geographic Science, Changchun Normal University, Changchun 130102, China
* Correspondence: fangchong@iga.ac.cn

Abstract: Nitrogen and phosphorus are limiting nutrients in freshwater ecosystems, and the remote estimation of total phosphorus (TP) and total nitrogen (TN) in eutrophic waters is of great significance. This study utilized machine learning algorithms based on Sentinel-2 satellite imagery for remote estimation of TP and TN concentrations in Lake Xingkai, Chagan and Songhua. Results indicate that random forest (RF) and XGBoost regression algorithms perform better. The performance of the GBDT algorithm was slightly lower than that of the RF and XGBoost regression algorithms, the BP algorithm had overfitting, and the SVR algorithm had poor fitting performance. Results showed that the TN concentration inversion model based on the RF algorithm had the highest accuracy (R^2 = 0.98, RMSE = 0.09, MAPE = 19.74%). The Extreme Gradient Boosting (XGB) model also performed well, though slightly less accurately than RF (R^2 = 0.97, RMSE = 0.14, MAPE = 20.67%). For TP concentration, the XGB model's performance (R^2 = 0.82, RMSE = 0.08, MAPE = 24.89%) was comparable to that of the RF model (R^2 = 0.82, RMSE = 0.07, MAPE = 29.55%). The RF algorithm was applied to all cloud-free Sentinel-2 satellite images of these typical lakes in northeastern China during the non-glacial period from 2017 to 2023, generating spatiotemporal distribution maps of TP and TN concentrations. Between 2017 and 2023, TP concentrations in Lake Xingkai, Chagan and Songhua showed increasing, decreasing, and initially decreasing then increasing patterns, respectively. A positive correlation between temperature and TP concentration was observed, as higher temperatures enhance biological activity. In contrast, a negative correlation was found with TN concentration, as higher temperatures promote phytoplankton growth and reproduction. This study not only offers a new method for monitoring eutrophication in lakes but also provides valuable support for sustainable water resource management and ecological protection goals.

Keywords: total nitrogen; total phosphorus; remote sense; machine learning

check for updates

Academic Editors: SeungHyun Son and Teodosio Lacava

Received: 12 December 2024
Revised: 28 December 2024
Accepted: 9 January 2025
Published: 13 January 2025

Citation: Qin, H.; Fang, C.; Liu, G.; Song, K.; Li, Z.; Li, S.; Tao, H.; Yan, Z. Temperature Is a Key Factor Affecting Total Phosphorus and Total Nitrogen Concentrations in Northeastern Lakes Based on Sentinel-2 Images and Machine Learning Methods. *Remote Sens.* **2025**, *17*, 267. https://doi.org/10.3390/rs17020267

Copyright: © 2025 by the authors. Licensee MDPI, Basel, Switzerland. This article is an open access article distributed under the terms and conditions of the Creative Commons Attribution (CC BY) license (https://creativecommons.org/licenses/by/4.0/).

1. Introduction

Lakes are integral components of the terrestrial hydrosphere, providing critical support for human sustenance, industrial operations, and recreational activities, while also playing a vital role in the preservation of biodiversity [1–3]. In recent decades, the eutrophication of lakes and reservoirs in China has accelerated significantly due to the combined

pressures of sewage discharge, nutrient enrichment, aquaculture practices, and climate change [4,5]. Population growth and accelerated economic development have led to significant environmental challenges in the lakes of northeastern China, exemplified by the occurrence of many algal bloom events in Lake Xingkai and Songhua Reservoir [6]. Aquatic environments with moderate to high levels of nutrients are beneficial for the formation of blue-green algae blooms. In contrast, diatom blooms exhibit greater sensitivity to elevated concentrations of phosphates and silicates [7]. Eutrophication, a serious phenomenon in water pollution, is characterized by the proliferation of algae and the excessive enrichment of nutrients in aquatic ecosystems [8]. According to research by the Organization for Economic Cooperation and Development (OECD), approximately 80% of water eutrophication is due to phosphorus, 10% is directly related to both nitrogen and phosphorus, and the remaining 10% is caused by nitrogen and other factors [9,10]. In lakes, nitrogen and phosphorus concentrations critically influence the growth and reproduction of phytoplankton [11–13]. The United Nations (UN) Sustainable Development Goals (SDGs) include targets for protecting water quality, emphasizing freshwater lakes, and monitoring key parameters such as nitrogen, phosphorus, pH, dissolved oxygen, and conductivity [14]. Consequently, TP and TN concentrations are vital chemical indicators for water quality monitoring. Accurate inversion of these concentrations is essential for effective monitoring, management, and protection of aquatic environments. To address the issue of eutrophication in large lakes, Sun et al. [15] combined spectral classification and support vector machine (SVM) methods to develop a remote sensing inversion model for TP concentration.

Traditional water quality monitoring methods often rely on on-site sampling and analysis, which require significant manpower, resources, and financial investment. Moreover, these methods typically have low monitoring frequencies and provide limited data, making it difficult to reflect the heterogeneity of macro scale spatiotemporal changes in water bodies [9,16]. Remote sensing technology offers a more advanced alternative that not only overcomes the shortcomings and deficiencies of traditional detection methods, but also enables comprehensive, efficient, low-cost, large-scale, and periodic monitoring of water environments [17].

In recent decades, advances in computer technology have facilitated the application of machine learning algorithms in satellite remote sensing for water quality assessment [18,19]. Common machine-learning methods include artificial neural networks, support vector machines, and random forests. Artificial neural networks, known for their distributed associative, self-learning, and self-organizing capabilities, are frequently used for data mining and predictive modeling. They have been widely applied in water quality parameter inversion and evaluation [20–22]. SVMs are primarily utilized in pattern recognition and handle data classification and regression problems by employing a supervised learning approach and the principle of statistical risk minimization, resulting in straightforward and interpretable outcomes [22–24]. As a widely utilized machine learning technique, random forest is a supervised algorithm that handles classification and regression. It constructs numerous decision trees using the bagging method, selects random training samples, and chooses features from all input variables to optimize feature selection and node splitting. The ultimate classification is decided by a majority vote among the decision trees [25,26]. The random forest algorithm's strength lies in its ability to determine the relative significance of each feature in prediction by examining the number of nodes connected to each feature [27]. As a result, machine learning models offer promising and reliable methods for estimating TP and TN concentrations in optically complex inland waters.

The Northeast Lake region considered in this study includes Lake Xingkai, Lake Chagan, and Lake Songhua, all located in a high-altitude inland cold zone. These lakes have

experienced a decline in water quality over the past few years, with increasing frequency and intensity of harmful algal blooms [28–30]. To perform a thorough examination of variations in TP and TN levels, this study focuses on the following objectives: (1) establishing a remote sensing inversion model for TP and TN concentrations in the Northeast Lake area using machine learning algorithms; (2) assessing the temporal and spatial development of TP and TN concentrations from 2017 to 2023 using data from Sentinel-2 images; and (3) exploring the spatiotemporal variability in TP and TN concentrations and the driving mechanisms of climate parameters. Through these studies, we intend to develop a thorough understanding of the changes in TP and TN levels in the Northeast Lake area, which will serve as a scientific basis for the management and protection of lake ecosystems.

2. Materials and Methods

2.1. Study Area

This study focused on three lakes: Xingkai Lake, Chagan Lake, and Songhua Lake, which are distributed across different latitudes, altitudes, and climate zones (refer to Figure 1). Xingkai Lake is located in a mid-temperate monsoon climate zone, whereas Chagan Lake and Songhua Lake are situated in temperate continental monsoon climate zones. Xingkai Lake (44°27′–45°23′N, 131°58′–132°52′E) spans the international border between Russia and China, divided by a natural barrier into Daxingkai Lake and Xiaoxingkai Lake. Approximately one-quarter of Daxingkai Lake's surface area (1080 km^2) belongs to China, while the remainder (3080 km^2) is part of Russia. The total surface areas of Daxingkai Lake and Xiaoxingkai Lake are approximately 4160 km^2 and 176 km^2, respectively, with an elevation of 69 m and an average depth of 1.8 m. The region receives an average annual precipitation of about 566 mm [31,32]. Xingkai Lake typically thaws in mid-to-late April and freezes in mid-November, with an average annual temperature of approximately 3 °C.

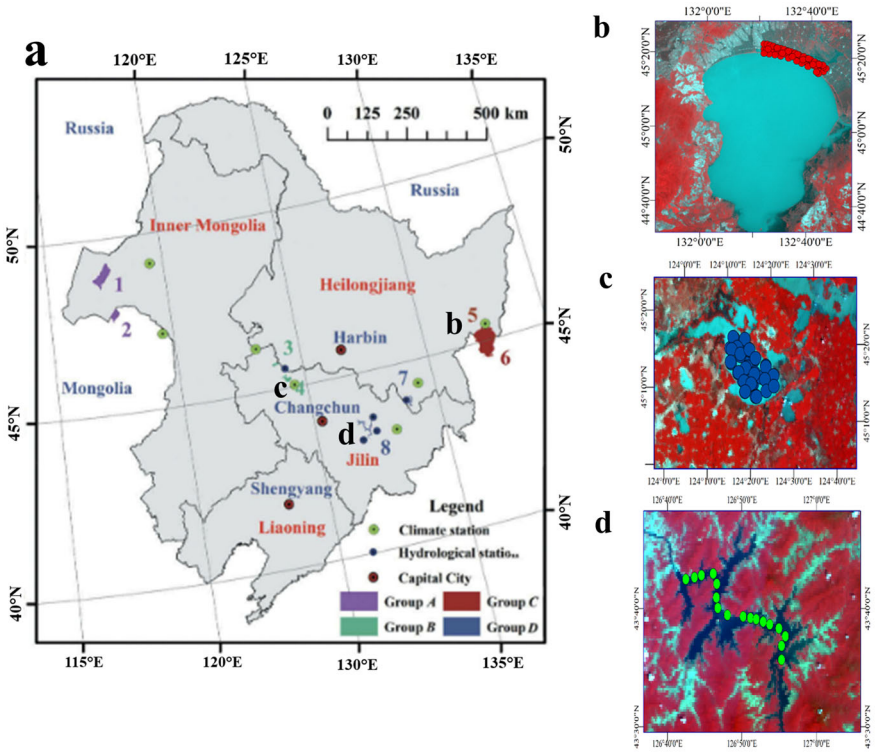


Figure 1. (**a**) Geographical locations of Xingkai Lake, Songhua Lake, and Chagan Lake. (**b**) Distribution of sampling points in Xingkai Lake. (**c**) Distribution of sampling points in Songhua Lake. (**d**) Distribution of sampling points in Chagan Lake.

Chagan Lake (45°09′–45°30′N, 124°03′–124°34′E) is one of the largest freshwater lakes in northeastern China [33]. It covers a surface area of approximately 307 km^2, has an elevation of 126 m, and an average depth of 2.5 m. Annual precipitation ranges from 400 to 500 mm. The lake has a relatively long freezing period, with ice forming in mid-to-late November and breaking up in early April of the following year. The average annual temperature is around 4–5 °C.

Songhua Lake (43°08′–43°48′N, 126°37′–127°02′E) is located in Jilin Province. The lake has a narrow and elongated shape, with a maximum width of 10 km and a total area of 554 km^2. It sits at an elevation of 266 m and has an average depth of 22 m. The thawing period begins in early April, and the lake typically freezes in mid-November. The average annual temperature ranges between 3–4 °C.

2.2. Data Sources and Processing

2.2.1. Field Sampling and Laboratory Analysis

This study conducted eight field investigations and collected a total of 131 water samples from the three study lakes between 2021 and 2022 (Table 1) to establish TP (total phosphorus) and TN (total nitrogen) concentration inversion models. All water samples were collected from a depth of 0 to 20 cm. To determine the concentration of TP, the sample was filtered through a 0.45 μm microporous membrane. Subsequently, the TP concentration was measured using continuous flow analysis (CFA) and ammonium molybdate spectrophotometry, in accordance with the Chinese standard [34]. Similarly, following the Chinese standard, a specified volume of raw water was filtered through a 0.45 μm microporous membrane, and the TN concentration was assessed using continuous flow analysis and naphthyl ethylenediamine dihydrochloride spectrophotometry [34].

Table 1. Field investigation collection date, lakes, and number of water samples.

Number	Date	Songhua Lake	Xingkai Lake	Chagan Lake	TP	TN
1	18 August 2021		10		10	10
2	1 September 2021			20	20	20
3	17 September 2021			19	19	19
4	28 September 2021			9	9	9
5	11 October 2021		18		18	18
6	22 October 2021		19		19	19
7	23 October 2021		18		18	18
8	21 September 2022	18			18	18
	Total	18	65	48		

2.2.2. Remote Sensing Data

The Multi-Spectral Imager (MSI) onboard the Sentinel-2A and Sentinel-2B satellites is well-suited for monitoring inland lakes, featuring 13 spectral bands in the visible to near-infrared range (400–2400 nm) with a spatial resolution of 10–60 m and a revisit period of 5 days [35]. The remote sensing data used in this study were obtained from the Google Earth Engine (GEE) platform (https://code.earthengine.google.com). Atmospheric correction was performed using the QA band provided by GEE, which showed a high degree of consistency with in situ spectral reflectance measurements [36,37]. Sentinel-2 full-resolution data, covering multiple high-quality cloud-free images of the study area from May 2017 to October 2023, were analyzed.

Following data quality inspection, 122 samples were selected for further processing. Data verification criteria included (1) ensuring that samples were not collected during algal bloom events to avoid anomalies; (2) matching with high-quality Sentinel-2 images, remov-

ing clouds, shadows, and land signals to ensure quality and meet analysis requirements; and (3) maintaining a temporal gap of no more than 48 h between sample collection and image acquisition to ensure spatiotemporal consistency and accuracy.

2.2.3. Lake Masks and Environmental Parameters

Lake boundaries were used to mask TP and TN concentration distribution maps derived from Sentinel-2 image data. The Normalized Difference Water Index (NDWI) threshold segmentation method was employed to delineate water body boundaries [38]. To mitigate the influence of algal blooms and aquatic vegetation on inversion results, the Normalized Difference Vegetation Index (NDVI) was used to exclude abnormal pixels [39]. Additionally, we buffered 2 pixels (600 m) inward from the extracted lake boundary as the water boundary of the lake to avoid mixed pixels and proximity effects.

Meteorological data for the lakes were obtained from the Resource and Environmental Science Data Platform (https://www.resdc.cn). These data included daily temperature (°C), wind speed (m/s), sunshine duration (hours), air pressure (kPa), and precipitation (mm) from 2017 to 2021. These values were averaged to derive monthly mean temperature (TEM), average wind speed (WIN), annual sunshine duration (SSD), mean atmospheric pressure (PRS), and mean precipitation (PRE).

2.3. Machine Learning Methods

In the course of this research, we used machine learning (ML) algorithms to construct models for estimating TN and TP concentrations in different lakes. Five commonly used machine learning models were compared, including Extreme Gradient Boosting (XGBoost), Support Vector Regression (SVR), Backpropagation Neural Network (BP), Gradient Boosting Decision Tree (GBDT), and Random Forest (RF). Model development is a key step in effectively utilizing remote sensing data to estimate the concentrations of TN and TP in lakes [40–44].

Various combinations of surface reflectance (SR) from different Sentinel-2 image bands were used as input variables, with TN and TP concentrations as output values (Table 2). Spearman correlation analysis indicated a strong correlation ($r > 0.4$) between TN concentration and the ultra-blue band B1 (443 nm), red-edge band B6 (740 nm), red-edge band B7 (783 nm), and red-edge band B8 (842 nm). Based on this analysis, the following band combinations were identified as sensitive input variables for TN concentration: B1 − B6, B1 − B8, (B1 − B6)/(B1 + B6), B1 − B7, B1 − B4, (B1 − B4)/(B1 + B4), (B1 − B7)/(B1 + B7), and B1–B5, where "B" represents different Sentinel-2 bands.

Table 2. Selected spectral bands and band combinations for modeling.

Spectral Band	TN	TP
Basic Bands	B1, B6, B7, B8	B3, B6, B8, B8A
Band Combinations	B1 − B6, B1 − B8, (B1 − B6)/(B1 + B6), B1 − B7, B1 − B4, (B1 − B4)/(B1 + B4), (B1 − B7)/(B1 + B7), B1 − B5	B8 − B8A, B6 − B8A, (B5 + B8)/(B5 − B8), (B5 + B6)/(B5 − B6), B5/B5 − B8, B5/B5 − B6, (B3 + B8A)/(B3 − B8A)

Similarly, Spearman correlation analysis showed a strong correlation ($r > 0.4$) between TP concentration and red-edge band (B5, 705 nm), red-edge band (B6, 740 nm), red-edge band (B8, 842 nm), and near-infrared band (B8A, 865 nm). The following band combinations were therefore identified as sensitive input variables for TP concentration: B8–B8A, (B5 + B8)/(B5 − B8), (B5 + B6)/(B5 − B6), B5/(B5 − B8), B5/(B5 − B6), B6 − B8A, and (B3 + B8A)/(B3 − B8A). The selected bands and their combinations for the final inversion models are presented in Table 2. Figure 2 illustrates the technical framework for inverting TN and TP concentrations using Sentinel-2 images.

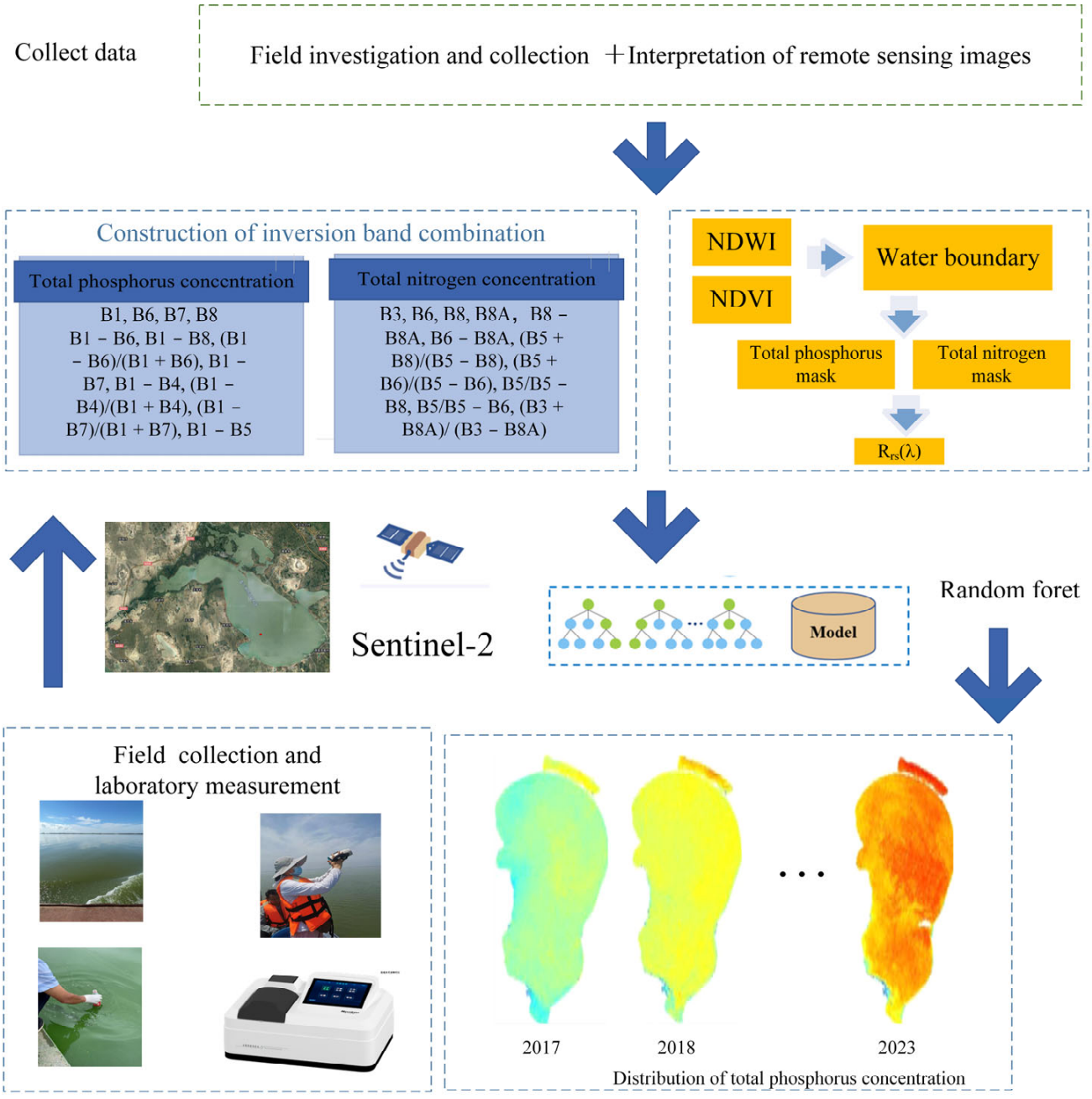


Figure 2. Framework of TN and TP concentration inversion models based on Sentinel-2 images.

2.4. Statistical Analysis and Accuracy Evaluation

Statistical analysis was performed using IBM SPSS Statistics 26 software, including Pearson correlation (represented by the correlation coefficient, r), analysis of variance (ANOVA), and regression analysis. The model's predictive accuracy was evaluated using

the coefficient of determination (R^2), root mean square error (RMSE), and mean absolute percentage error (MAPE) [45,46]. The formulas for these metrics are as follows:

$$R^2 = 1 - \frac{\sum_{i=1}^{N}\left(y_i' - y_i\right)^2}{\sum_{i=1}^{N}\left(y_i - y\right)^2} \quad (1)$$

$$RMSE = \sqrt{\frac{\sum_{i=1}^{N}\left(y_i' - y_i\right)^2}{N}} \quad (2)$$

$$MAPE = \frac{1}{N}\sum_{i=1}^{N}\left|\frac{y_i' - y_i}{y_i}\right| \times 100\% \quad (3)$$

where N represents the number of samples, and y_i' and y_i are the predicted and observed values, respectively. The coefficient of determination (R^2) indicates the proportion of variance as a predictive performance explained by the model, while RMSE and MAPE assess the consistency between observed and predicted values.

3. Results

3.1. Calibration and Validation of the TN and TP Algorithm

The selected feature bands in Section 2.3 are used as input variables to construct an inversion model for TN concentration and TP concentration. The total sample data (N = 122) were randomly divided into two parts: two-thirds (N = 82) of the sampling points were used as the training dataset for model construction and parameter adjustment. The remaining one-third (N = 40) of the data was allocated to validate the accuracy of the model.

Different machine learning methods show significant differences in constructing inversion models for TN concentration and TP concentration. Overall, the RF and XGBoost regression algorithms perform better. The GBDT algorithm is slightly inferior to the RF and XGBoost regression algorithms, the BP algorithm has overfitting, and the SVR algorithm has poor fitting performance. Results showed that the RF TN concentration model exhibited stable performance (R^2 = 0.98, RMSE = 0.09, and MAPE = 19.74%). The observed on-site measurements align well with the values predicted by the RF model, and the data points are evenly positioned around the 1:1 line. In contrast, the performance of XGB's TN concentration model is slightly lower (R^2 = 0.97, RMSE = 0.14, and MAPE = 20.67%). The TP concentration model of RF performs well (R^2 = 0.82, RMSE = 0.07, and MAPE = 29.55%). The observed on-site measurements and RF model predictions are highly consistent (refer to Figure 3). The performance of the XGB model is comparable to that of the RF model (R^2 = 0.82, RMSE = 0.08, and MAPE = 24.89%). The data derived from the RF and XGB models for TN and TP concentrations were analyzed using SPSS to conduct a paired *t*-test. The results indicated that the significance levels for TN (α = 0.652) and TP (α = 0.178) both exceeded the threshold of 0.05, suggesting that there was no statistically significant difference. This study used 5-fold cross validation to cross validate the RF and XGB models. The dataset was divided into five equally large subsets, with four subsets selected for training and one subset for validation in each iteration. The procedure was carried out five times, with each subset serving as a validation set once, thus helping to find the optimal combination of hyperparameters.

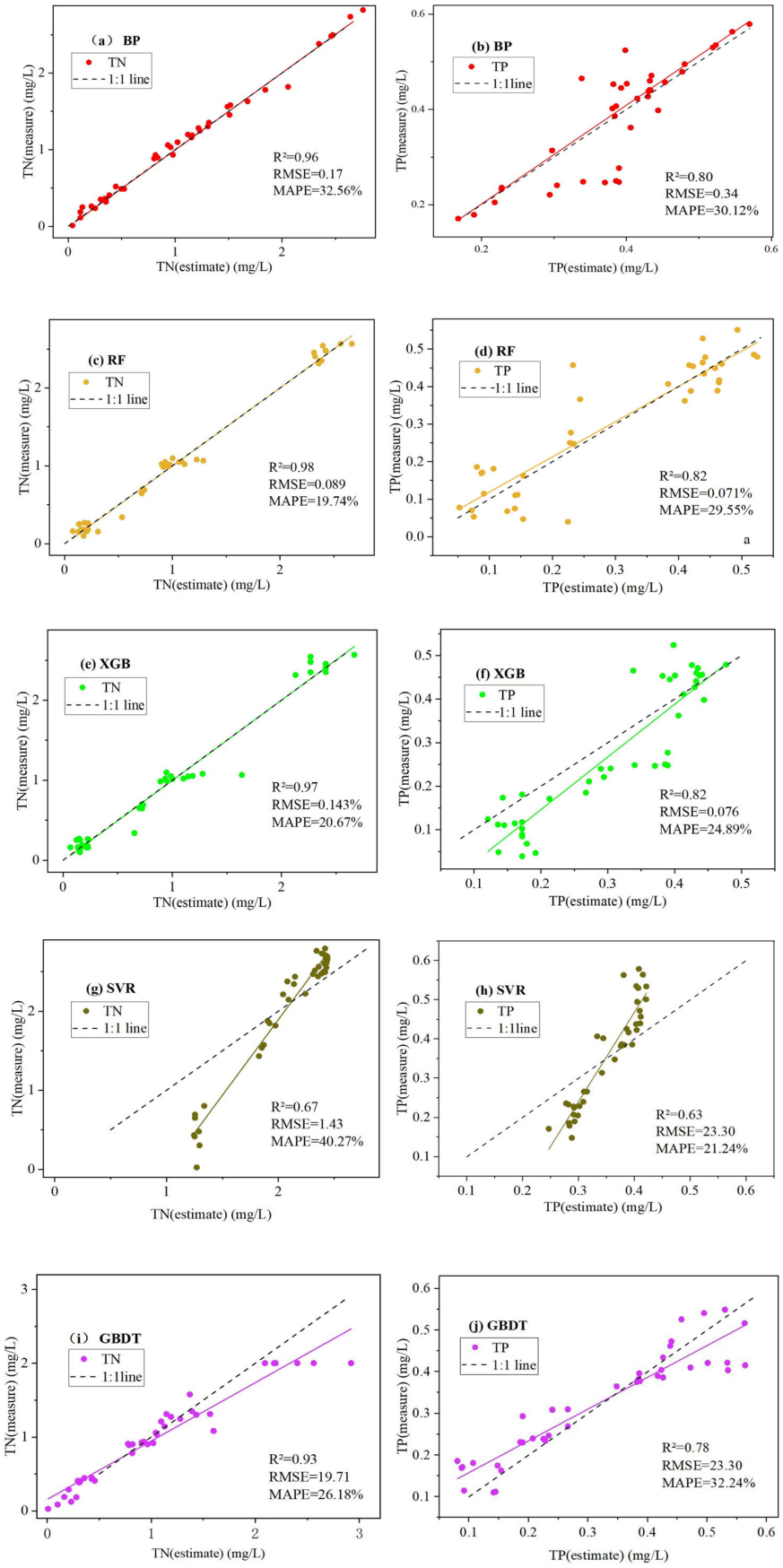


Figure 3. The relationship between the training values of backpropagation neural networks (BP) (**a**,**b**), random forests (RF) (**c**,**d**), extreme gradient boosting (XGBoost) (**e**,**f**), support vector regression (SVR) (**g**,**h**), and gradient boosting decision trees (GBDT) (**i**,**j**) and the corresponding actual measurement values.

3.2. Interannual Variations in TN and TP Concentrations

Utilizing the previously discussed Random Forest (RF) model, the inversion results for TN and TP concentrations were computed. Subsequently, the layout in spatial terms of changes in TN and TP levels in Xingkai Lake (refer to Figure 4) and Chagan Lake (refer to Figure 5) were mapped for the period from May 2017 to October 2023. The findings revealed substantial spatial and interannual variability across all lakes.

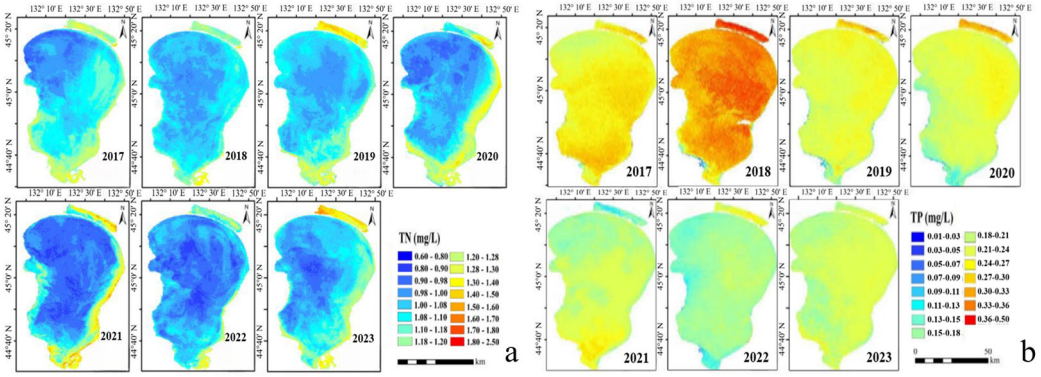


Figure 4. Distribution of TN concentration in Xingkai Lake (**a**) and TP concentration in Xingkai Lake (**b**).

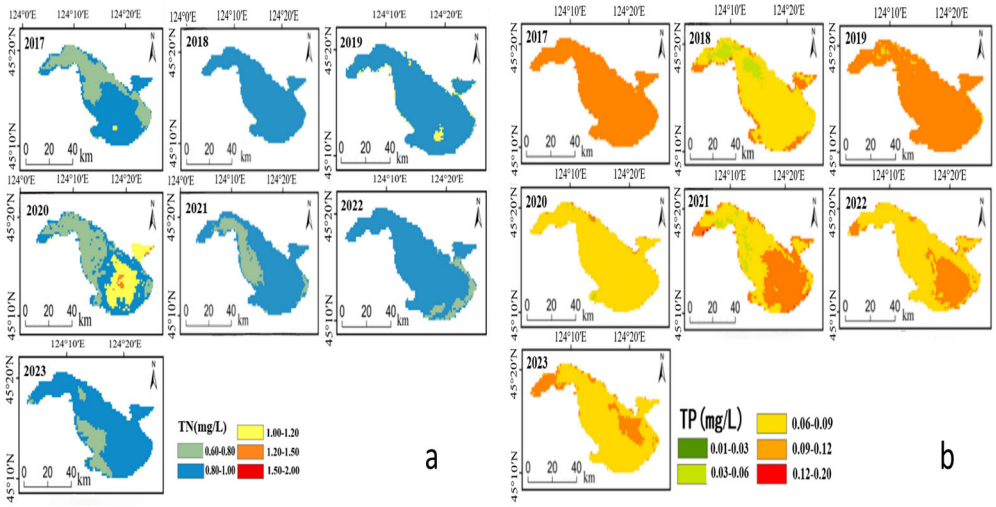


Figure 5. Distribution of TN concentration in Chagan Lake (**a**) and TP concentration in Chagan Lake (**b**).

Xingkai Lake:

TN Concentration Changes: Based on Sentinel-2 satellite remote sensing images, the estimated annual average TN concentration from 2017 to 2023 ranged from 0.6 to 2.5 mg/L (refer to Figure 4a). Between 2017 and 2019, TN concentrations in XiaoXingkai Lake were significantly higher than those in Daxingkai Lake. No substantial north–south differentiation in TN concentrations was observed throughout Xingkai Lake in most years. However, east–west differentiation was evident in 2017, 2018, and 2023, showing a trend of lower concentrations in the west and higher concentrations in the east.

TP Concentration Changes: Based on Sentinel-2 satellite remote sensing images, the estimated annual average TP concentration from 2017 to 2023 ranged from 0.01 to 0.50 mg/L (see Figure 4b). The annual average TP concentration in Xingkai Lake has shown fluctuations and an overall increase since 2017. In 2019, the TP concentration decreased to 0.168 mg/L. Subsequently, in 2020 and 2022, it increased by 0.022 mg/L and

0.036 mg/L, respectively, relative to the preceding year. In 2023, the TP concentration attained its maximum level, measuring 0.322 mg/L. In most years, the TP concentrations in Xiaoxingkai Lake were comparable to those in Daxingkai Lake, except for 2018 and 2020, when TP concentrations in Xiaoxingkai Lake were significantly higher. No distinct north–south differentiation was observed between 2017 and 2023, while east–west differentiation was observed in 2017, 2022, and 2023, showing a trend of concentrations higher in the west and lower in the east. The distribution of TP concentration exhibited relative uniformity in the years 2017, 2018, 2019, and 2020. Overall, the spatial pattern of TP concentrations in Xingkai Lake has shown significant changes from 2017 to 2023, with a general upward trend.

Chagan Lake:

TN Concentration Changes: Utilizing Sentinel-2 satellite remote sensing imagery, the estimated annual average TN concentration for the period from 2017 to 2023 ranged from 0.6 to 2.0 mg/L (refer to Figure 5a). Analyzing the temporal pattern of annual average TN concentrations across the entire Chagan Lake from 2017 to 2023 revealed a marked increase in TN concentration in the year 2020. Throughout most years, there was no significant north–south differentiation in the TN concentration between the northern and southern waters of Chagan Lake. However, an exception occurred in 2017, when lower concentrations were observed in the north and higher concentrations in the south. In contrast, east–west differentiation became evident in 2020, 2021, and 2023, with a pronounced trend of lower concentrations in the west and higher concentrations in the east.

TP Concentration Changes: Utilizing Sentinel-2 satellite remote sensing imagery, the estimated annual average total phosphorus (TP) concentration for the period from 2017 to 2023 ranged from 0.01 to 0.20 mg/L (see Figure 5b). Since 2017, the annual average TP concentration across Chagan Lake has exhibited fluctuations, with an overall decreasing trend. No significant differentiation between the northern and southern regions was observed during this period. However, spatial disparities between the eastern and western regions were evident in certain years, notably in 2021 and 2022, where a pronounced trend of lower concentrations in the west and higher concentrations in the east was observed. Overall, the concentration distribution remained relatively uniform across the majority of the lake. In conclusion, the spatial distribution of the mean total phosphorus (TP) concentration in Chagan Lake has undergone significant alterations from 2017 to 2023, exhibiting an overall trend of fluctuating decline.

Songhua Lake:

TN Concentration Changes: Based on Sentinel-2 satellite remote sensing images, the estimated annual average TN concentration from 2017 to 2023 ranged from 0.6 to 2.7 mg/L. The annual average TN concentration increased sharply in 2018, and since 2019, it has shown a fluctuating but generally rising trend. No significant north–south differentiation was observed from 2017 to 2023.

TP Concentration Changes: Based on Sentinel-2 satellite remote sensing images, the estimated annual average TP concentration from 2017 to 2023 ranged from 0.01 to 1.00 mg/L. From 2020, TP concentrations fluctuated, initially decreasing and then increasing year by year. No significant north–south differentiation was observed from 2017 to 2023. Overall, the spatial pattern of TP concentrations in Songhua Lake has shown significant changes from 2017 to 2023, with a general trend of initial decrease followed by an increase.

4. Discussion

4.1. Analysis of Driving Factors

Relationship Between Meteorological Factors and TN and TP Concentrations

TN and TP concentrations exhibit significant heterogeneity at both temporal and spatial scales. To understand the potential influence of climatic factors on TN and TP concentrations in typical lakes in northeastern China, we calculated the Spearman correlation coefficients and corresponding significance test *p*-values for wind speed (WIN), temperature (TEM), sunshine duration (SSD), atmospheric pressure (PRS), and precipitation (PRE) from 2017 to 2021 (refer to Figure 6).

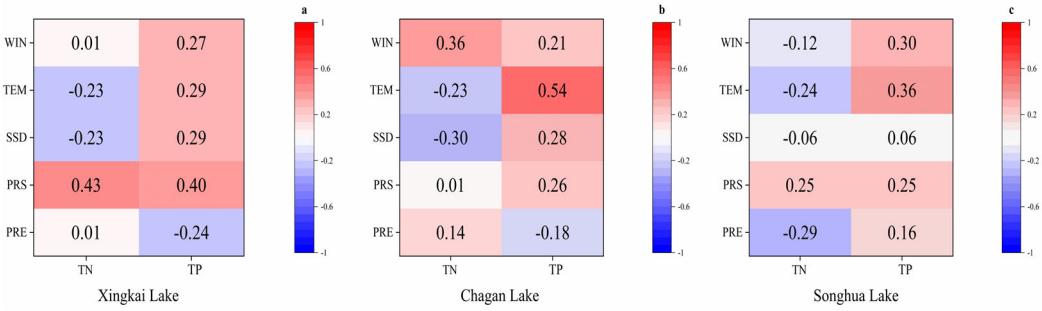


Figure 6. Relationship between water quality parameters in Xingkai Lake (**a**), Chagan Lake (**b**), and Songhua Lake (**c**).

The findings indicate that in Xingkai Lake, PRS exhibits a statistically significant moderate positive correlation with both TN and TP concentrations (r = 0.43, $p < 0.01$; r = 0.40, $p < 0.01$, respectively). Conversely, TEM and SSD demonstrate a statistically significant but weak negative correlation with TN concentration (r = −0.23, $p < 0.01$ for both) but weakly positively correlation with TP concentration (r = 0.29, $p < 0.01$ for both) (refer to Figure 7). This may be because higher temperatures significantly increase the release of phosphorus and stimulate biological activity. Xingkai Lake, being a typical shallow water body, experiences sediment disturbance due to biological growth, leading to the release of phosphorus from suspended particulate matter and sediment, as indicated in previous studies [33,45]. Furthermore, the optimal temperature range for cyanobacterial growth is between 25 °C and 30 °C. Consequently, within this temperature range, the growth and reproduction rates of phytoplankton are enhanced. In comparison to phosphorus, phytoplankton frequently exhibit higher nitrogen consumption, thereby increasing the utilization efficiency of TN [47,48]. The correlations between WIN, PRE, and TN concentrations are low (r = −0.01 and r = 0.01, respectively). However, there is a weak positive correlation between WIN and TP concentration (r = 0.27, $p < 0.01$). Wind-induced disturbances can resuspend a large amount of sediment in a short time, increasing the phosphorus content in the water [49]. PRE shows a weak negative correlation with TN concentration (r = −0.24, $p < 0.01$). Precipitation exerts both erosion and dilution effects. Erosion can cause pollutants to move from their original location into water bodies via runoff, whereas dilution reduces the concentration of pollutants within the water. The balance between these forces varies, which may either increase or decrease pollutant concentrations. When rainfall is low, producing no surface runoff, rainwater entering the water body dilutes and reduces TN concentrations. Conversely, heavy rainfall generates surface runoff, which can carry pollutants from farmland, aquaculture, and domestic sources into the water body. If the erosion effect outweighs the dilution effect, the TN concentration increases [50–52].

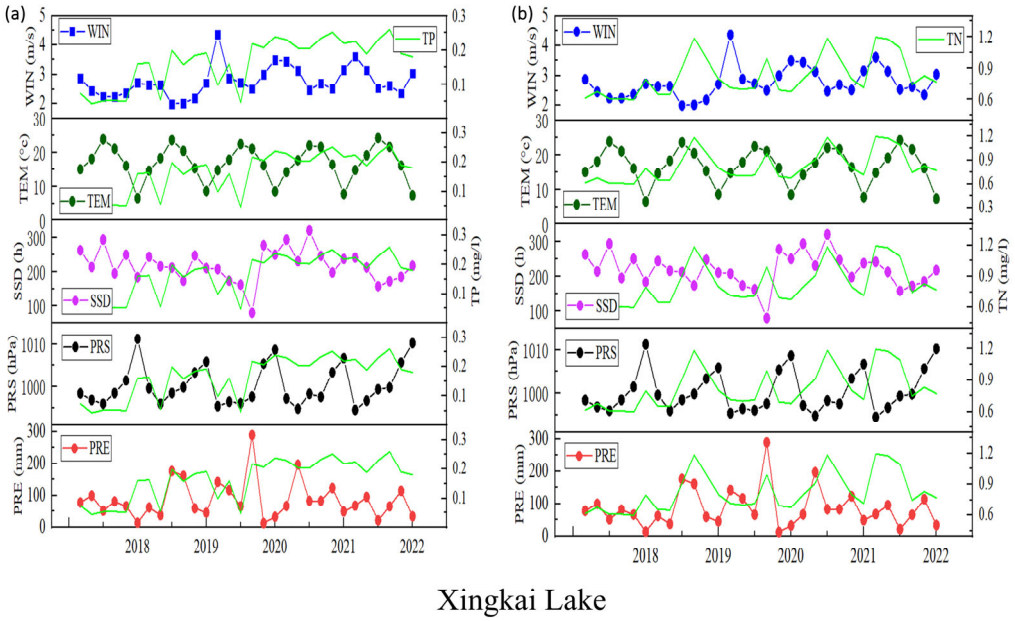


Figure 7. Distribution of TP concentration (**a**), TN concentration (**b**), and climate factors in Xingkai Lake.

The situation in Chagan Lake is generally similar to that in Xingkai Lake (refer to Figure 8). However, Songhua Lake differs slightly due to its greater depth, which limits the sunlight's impact on plant photosynthesis. Therefore, there is no significant correlation between SSD and TN or TP concentrations in this lake (refer to Figure 9). PRS shows a weak positive correlation with TN and TP concentrations ($r = 0.25$, $p < 0.01$ for both), potentially due to changes in air pressure affecting temperature through adiabatic processes, weather systems, and atmospheric stability mechanisms, thereby impacting phytoplankton growth and TN and TP concentrations [53,54].

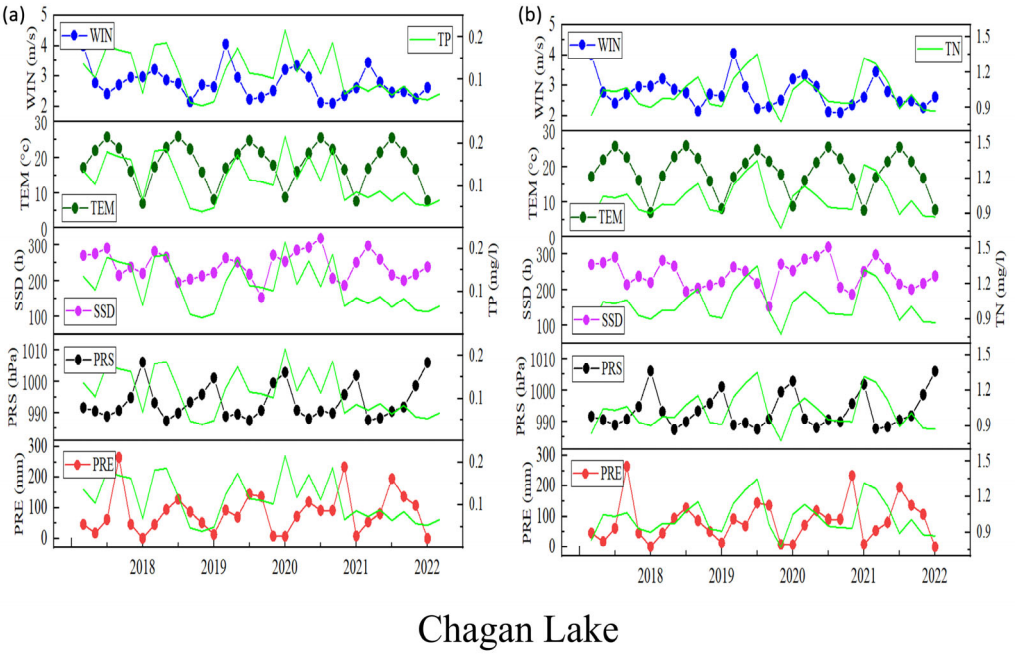


Figure 8. Distribution of TP concentration (**a**), TN concentration (**b**), and climate factors in Chagan Lake.

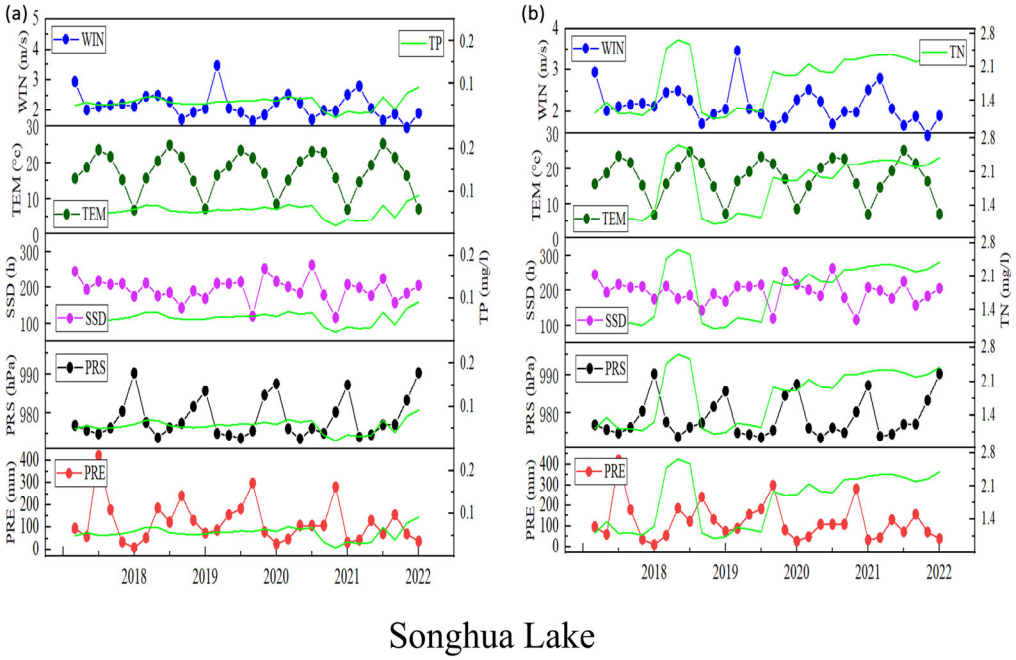


Figure 9. Distribution of TP concentration (**a**), TN concentration (**b**), and climatic factors in Songhua Lake.

In conclusion, the growth of phytoplankton in aquatic environments is influenced both directly and indirectly by factors such as TEM, SSD, and PRS, which in turn affect the concentrations of total nitrogen (TN) and total phosphorus (TP) in lake ecosystems. Additionally, heavy rainfall events generate surface runoff that transports pollutants from agricultural, aquacultural, and domestic sources into water bodies, further influencing TN and TP levels [53,54]. The movement of nutrients, pollutants, and particulates is predominantly governed, or at least influenced, by horizontal wind-driven flows [55]. Nevertheless, the various natural elements are intricately interconnected and not entirely independent. Consequently, there is significant potential to investigate additional factors or the interactions among these natural elements to predict changes in TN and TP concentrations in lakes under climate change scenarios.

4.2. Applicability and Uncertainty of the Model

The RF algorithm is a well-known and powerful method in machine learning. In this study, we constructed TN and TP concentration inversion models for different lakes using the RF algorithm. Our method successfully estimated TN and TP concentrations in Xingkai Lake, Chagan Lake, and Songhua Lake. The quality of the training dataset plays a crucial role in determining the RF model's performance. Insufficient or unrepresentative samples may lead to overfitting or underfitting, resulting in poor robustness [43,56]. Therefore, the training dataset should be comprehensive and representative, covering various conditions within the target area. Our study focused only on the connection between TN and TP levels and spectral bands, without considering how other water quality parameters might impact inversion results. Future research should consider these additional factors to improve the model's predictive accuracy and generalization ability, thereby enhancing its performance in practical applications.

4.3. Implications for Environmental Management

Understanding the trends in TN and TP concentrations in lakes is crucial for managing inland aquatic ecosystems [57,58]. This study provides a detailed analysis of changes in TN and TP concentrations in cold lakes over a long-term period, offering new insights and

data support. The analysis methods applied have broad applications for future research: (1) achieving more precise estimation of TN and TP concentrations, thus improving the accuracy of lake water quality assessments; (2) exploring the spatiotemporal variability in TN and TP concentrations in different lakes, which is essential for controlling eutrophication in lakes, reservoirs, and other water bodies, thereby enhancing water quality disaster warning and pollution control efforts; and (3) predicting changes in TN and TP concentrations in lakes under climate change scenarios, thereby providing a scientific basis for environmental protection and policy formulation.

Managing lakes becomes more difficult due to the significant threat posed by algal blooms [43]. The prediction of TN and TP concentrations in the context of climate change, alongside the development of specialized climate models for the monitoring of eutrophication in lacustrine environments, holds significant potential. For example, changes in precipitation will affect how long water stays and how nutrients are retained. As a result, shifts in TN and TP levels in lakes might be deduced from alterations in precipitation [59,60]. Understanding the dynamic changes in TN and TP concentrations is essential for effective lake management. Long-term observation of TN and TP concentrations, combined with remote sensing data, can provide valuable support for decision-making by lake managers and serve as a solid scientific basis for formulating targeted management strategies, ultimately improving the ecological health of lakes.

5. Conclusions

The objective of this research was to create an effective model using machine learning techniques to predict TN and TP levels in inland cold lakes with intricate optical characteristics. A TN and TP concentration inversion model was constructed using Sentinel-2 satellite images. The results indicate that RF and XGBoost regression algorithms perform better. The GBDT algorithm showed slightly lower performance than the RF and XGBoost regression algorithms, the BP algorithm has overfitting, and the SVR algorithm has poor fitting performance. For TN concentration, the RF model demonstrated stable performance (R^2 = 0.98, RMSE = 0.09, and MAPE = 19.74%), showing strong agreement between in situ measurements and RF model predictions. The XGB model performed as well as the RF model (R^2 = 0.97, RMSE = 0.14, and MAPE = 20.67%).

For TP concentration, the XGB model exhibited stable performance (R^2 = 0.82, RMSE = 0.08, and MAPE = 24.89%), with good agreement between in situ measurements and XGB model predictions. In comparison, the RF model showed slightly lower performance for TP concentration (R^2 = 0.82, RMSE = 0.07, and MAPE = 29.55%). Overall, the RF model effectively inverted the TN and TP concentrations of lakes in northeastern China from 2017 to 2023.

The results indicated that the TP concentration in Xingkai Lake generally exhibited an upward fluctuating trend over this period. In some years, the TN concentration displayed a more pronounced pattern of being lower in the west and higher in the east. In Chagan Lake, the spatial pattern of the average TP concentration changed significantly from 2017 to 2023, showing an overall fluctuating downward trend. The TN concentration did not show significant north–south differentiation, although a distinct pattern of lower concentrations in the west and higher concentrations in the east was observed in certain years. A significant trend in the spatial pattern of the average TP concentration in Songhua Lake was observed, with an initial decrease followed by an increase from 2017 to 2023.

Meteorological factors, especially temperature, were identified as key drivers affecting TN and TP concentrations in lakes in northeastern China. Suitable water temperatures were found to establish an environment conducive to algal growth, leading to increased

algal and phytoplankton proliferation, which in turn influenced TN and TP concentrations in the water.

The developed models not only accurately estimated TN and TP concentrations in lakes across northeastern China but also enhanced our understanding of their spatiotemporal distribution and changing trends. These findings provide critical support for water quality monitoring and ecological protection efforts. As new sensors are deployed in the future, this method has the potential to improve the identification of inland water bodies with complex optical characteristics, significantly enhancing our ability to monitor and manage eutrophication in aquatic ecosystems.

Author Contributions: H.Q.: conceptualization, data curation, formal analysis, methodology, visualization, writing—original draft. C.F.: funding acquisition, project administration, supervision, writing—review and editing. G.L.: funding acquisition, project administration, resources. K.S.: funding acquisition, project administration, resources. Z.L.: funding acquisition, project administration, investigation. S.L.: investigation, resources. H.T.: investigation, resources. Z.Y.: software, investigation. All authors have read and agreed to the published version of the manuscript.

Funding: The research was funded by the National Natural Science Foundation of China (42171374, 42101366), Natural Science Foundation of Jilin Province, China (YDZJ202401474ZYTS), Young Scientist Group Project of Northeast Institute of Geography and Agroecology, Chinese Academy of Sciences (2023QNXZ01), Youth Innovation Promotion Association of Chinese Academy of Sciences, China (2022228).

Data Availability Statement: Sentinel-2 data are openly available for download from the Google Earth Engine (GEE) platform, https://code.earthengine.google.com. Meteorological data were downloaded from the Resource and Environmental Science Data Platform, https://www.resdc.cn.

Conflicts of Interest: The authors declare no conflicts of interest.

References

1. Ho, J.C.; Michalak, A.M.; Pahlevan, N. Widespread Global Increase in Intense Lake Phytoplankton Blooms since the 1980s. *Nature* **2019**, *574*, 667–670. [CrossRef]
2. Casas-Ruiz, J.P.; Jakobsson, J.; del Giorgio, P.A. The Role of Lake Morphometry in Modulating Surface Water Carbon Concentrations in Boreal Lakes. *Environ. Res. Lett.* **2021**, *16*, 074037. [CrossRef]
3. Cao, Z.; Duan, H.; Feng, L.; Ma, R.; Xue, K. Climate- and Human-Induced Changes in Suspended Particulate Matter over Lake Hongze on Short and Long Timescales. *Remote Sens. Environ.* **2017**, *192*, 98–113. [CrossRef]
4. Fang, C.; Song, K.; Paerl, H.W.; Jacinthe, P.; Wen, Z.; Liu, G.; Tao, H.; Xu, X.; Kutser, T.; Wang, Z.; et al. Global Divergent Trends of Algal Blooms Detected by Satellite during 1982–2018. *Glob. Change Biol.* **2022**, *28*, 2327–2340. [CrossRef] [PubMed]
5. Hou, X.; Feng, L.; Tang, J.; Song, X.-P.; Liu, J.; Zhang, Y.; Wang, J.; Xu, Y.; Dai, Y.; Zheng, Y.; et al. Anthropogenic Transformation of Yangtze Plain Freshwater Lakes: Patterns, Drivers and Impacts. *Remote Sens. Environ.* **2020**, *248*, 111998. [CrossRef]
6. Fang, C. Water Quality Remote Sensing Inversion and Spatiotemporal Analysis on International Lake—A Case Study of Lake Xingkai. Ph.D. Thesis, Chinese Academy of Sciences, Changchun, China, 2020.
7. Fang, C.; Song, K.; Li, L.; Wen, Z.; Liu, G.; Du, J.; Shang, Y.; Zhao, Y. Spatial Variability and Temporal Dynamics of HABs in Northeast China. *Ecol. Indic.* **2018**, *90*, 280–294. [CrossRef]
8. Le, C.; Zha, Y.; Li, Y.; Sun, D.; Lu, H.; Yin, B. Eutrophication of Lake Waters in China: Cost, Causes, and Control. *Environ. Manag.* **2010**, *45*, 662–668. [CrossRef]
9. Du, C.; Wang, Q.; Li, Y.; Lyu, H.; Zhu, L.; Zheng, Z.; Wen, S.; Liu, G.; Guo, Y. Estimation of Total Phosphorus Concentration Using a Water Classification Method in Inland Water. *Int. J. Appl. Earth Obs. Geoinf.* **2018**, *71*, 29–42. [CrossRef]
10. Vollenweider, R. Phosphorus Loading Concept and Great Lakes Eutrophication. In *Phosphorus Management Strategies for Lakes: Proceedings of the 1979 Conference Sponsored by the New York State College of Agriculture and Life Sciences, a Statutory College of the State University at Cornell University, [and] the International Joint Commission (U.S. and Canada)*; Ann Arbor Science: Ann Arbor, MI, USA, 1979.
11. Xiong, J.; Lin, C.; Cao, Z.; Hu, M.; Xue, K.; Chen, X.; Ma, R. Development of remote sensing algorithm for total phosphorus concentration in eutrophic lakes: Conventional or machine learning? *Water Res.* **2022**, *215*, 118213. [CrossRef]

12. Xiong, J.; Lin, C.; Ma, R.; Cao, Z. Remote Sensing Estimation of Lake Total Phosphorus Concentration Based on MODIS: A Case Study of Lake Hongze. *Remote Sens.* **2019**, *11*, 2068. [CrossRef]
13. Gao, Y.; Gao, J.; Yin, H.; Liu, C.; Xia, T.; Wang, J.; Huang, Q. Remote Sensing Estimation of the Total Phosphorus Concentration in a Large Lake Using Band Combinations and Regional Multivariate Statistical Modeling Techniques. *J. Environ. Manag.* **2015**, *151*, 33–43. [CrossRef] [PubMed]
14. Shen, M.; Duan, H.; Cao, Z.; Xue, K.; Qi, T.; Ma, J.; Liu, D.; Song, K.; Huang, C.; Song, X. Sentinel-3 OLCI Observations of Water Clarity in Large Lakes in Eastern China: Implications for SDG 6.3.2 Evaluation. *Remote Sens. Environ.* **2020**, *247*, 111950. [CrossRef]
15. Sun, D.; Qiu, Z.; Li, Y.; Shi, K.; Gong, S. Detection of total phosphorus concentrations of turbid inland waters using a remote sensing method. *Water Air Soil Pollut.* **2014**, *225*, 1953. [CrossRef]
16. Cai, X.; Li, Y.; Lei, S.; Zeng, S.; Zhao, Z.; Lyu, H.; Dong, X.; Li, J.; Wang, H.; Xu, J.; et al. A Hybrid Remote Sensing Approach for Estimating Chemical Oxygen Demand Concentration in Optically Complex Waters: A Case Study in Inland Lake Waters in Eastern China. *Sci. Total Environ.* **2023**, *856*, 158869. [CrossRef]
17. Wimmer, A.; Markus, A.A.; Schuster, M. Silver Nanoparticle Levels in River Water: Real Environmental Measurements and Modeling Approaches—A Comparative Study. *Environ. Sci. Technol. Lett.* **2019**, *6*, 353–358. [CrossRef]
18. Chang, N.-B.; Xuan, Z.; Yang, Y.J. Exploring Spatiotemporal Patterns of Phosphorus Concentrations in a Coastal Bay with MODIS Images and Machine Learning Models. *Remote Sens. Environ.* **2013**, *134*, 100–110. [CrossRef]
19. Wang, J.; Cheng, S.; Jia, H.; Wang, Z.; Tang, U.W. An artificial neural network model for lake color inversion using TM imagery. *Huan Jing Ke Xue* **2003**, *24*, 73–76.
20. Chen, J.; Quan, W.; Cui, T.; Song, Q.; Lin, C. Remote Sensing of Absorption and Scattering Coefficient Using Neural Network Model: Development, Validation, and Application. *Remote Sens. Environ.* **2014**, *149*, 213–226. [CrossRef]
21. Concha, J.A.; Schott, J.R. Retrieval of Color Producing Agents in Case 2 Waters Using Landsat 8. *Remote Sens. Environ.* **2016**, *185*, 95–107. [CrossRef]
22. Boateng, E.Y.; Otoo, J.; Abaye, D.A. Basic Tenets of Classification Algorithms K-Nearest-Neighbor, Support Vector Machine, Random Forest and Neural Network: A Review. *J. Data Anal. Inf. Process.* **2020**, *8*, 341–357. [CrossRef]
23. Hearst, M.A.; Dumais, S.T.; Osuna, E.; Platt, J.; Scholkopf, B. Support Vector Machines. *IEEE Intell. Syst. Their Appl.* **1998**, *13*, 18–28. [CrossRef]
24. Cervantes, J.; Garcia-Lamont, F.; Rodríguez-Mazahua, L.; Lopez, A. A Comprehensive Survey on Support Vector Machine Classification: Applications, Challenges and Trends. *Neurocomputing* **2020**, *408*, 189–215. [CrossRef]
25. Sheykhmousa, M.; Mahdianpari, M.; Ghanbari, H.; Mohammadimanesh, F.; Ghamisi, P.; Homayouni, S. Support Vector Machine Versus Random Forest for Remote Sensing Image Classification: A Meta-Analysis and Systematic Review. *IEEE J. Sel. Top. Appl. Earth Obs. Remote Sens.* **2020**, *13*, 6308–6325. [CrossRef]
26. Li, X.; Ding, J.; Ilyas, N. Machine Learning Method for Quick Identification of Water Quality Index (WQI) Based on Sentinel-2 MSI Data: Ebinur Lake Case Study. *Water Supply* **2021**, *21*, 1291–1312. [CrossRef]
27. Belgiu, M.; Drăguţ, L. Random Forest in Remote Sensing: A Review of Applications and Future Directions. *ISPRS J. Photogramm. Remote Sens.* **2016**, *114*, 24–31. [CrossRef]
28. Xu, S.; Li, S.; Tao, Z.; Song, K.; Wen, Z.; Li, Y.; Chen, F. Remote Sensing of Chlorophyll-a in Xinkai Lake Using Machine Learning and GF-6 WFV Images. *Remote Sens.* **2022**, *14*, 5136. [CrossRef]
29. Qiang, S.; Song, K.; Shang, Y.; Lai, F.; Wen, Z.; Liu, G.; Tao, H.; Lyu, Y. Remote Sensing Estimation of CDOM and DOC with the Environmental Implications for Lake Khanka. *Remote Sens.* **2023**, *15*, 5707. [CrossRef]
30. Shi, X.; Gu, L.; Jiang, T.; Zheng, X.; Dong, W.; Tao, Z. Retrieval of Chlorophyll-a Concentrations Using Sentinel-2 MSI Imagery in Lake Chagan Based on Assessments with Machine Learning Models. *Remote Sens.* **2022**, *14*, 4924. [CrossRef]
31. Ji, X.; Liu, T.; Liu, J.; Li, J.; Pan, B. Investigation and Study on Water Quality and Pollution Condition in Lake Xingkai of China. *Environ. Monit. China* **2013**, *29*, 79–84.
32. Sun, D.; Sun, X. Hydrological Characteristics of Xingkai Lake. *Water Resour. Hydropower Northeast China* **2006**, *24*, 21.
33. Zhu, L.; Yan, B.; Wang, L.; Pan, X. Mercury Concentration in the Muscle of Seven Fish Species from Chagan Lake, Northeast China. *Environ. Monit. Assess.* **2012**, *184*, 1299–1310. [CrossRef] [PubMed]
34. Water quality Determination of Phosphate and Total Phosphorus Continuous Flow—Ammonium Molybdate Spectrophotometric mMethod. Available online: https://www.mee.gov.cn/ywgz/fgbz/bz/bzwb/jcffbz/201311/t20131106_262958.shtml (accessed on 19 December 2024).
35. Liang, Y.; Yin, F.; Xie, D.; Liu, L.; Zhang, Y.; Ashraf, T. Inversion and Monitoring of the TP Concentration in Taihu Lake Using the Landsat-8 and Sentinel-2 Images. *Remote Sens.* **2022**, *14*, 6284. [CrossRef]
36. Orusa, T.; Viani, A.; Cammareri, D.; Borgogno Mondino, E. A Google Earth Engine Algorithm to Map Phenological Metrics in Mountain Areas Worldwide with Landsat Collection and Sentinel-2. *Geomatics* **2023**, *3*, 221–238. [CrossRef]
37. Long, X.; Li, X.; Lin, H.; Zhang, M. Mapping the Vegetation Distribution and Dynamics of a Wetland Using Adaptive-Stacking and Google Earth Engine Based on Multi-Source Remote Sensing Data. *Int. J. Appl. Earth Obs. Geoinf.* **2021**, *102*, 102453. [CrossRef]

38. Gao, B. NDWI—A Normalized Difference Water Index for Remote Sensing of Vegetation Liquid Water from Space. *Remote Sens. Environ.* **1996**, *58*, 257–266. [CrossRef]
39. Rouse, J.W.; Haas, R.H.; Schell, J.A.; Deering, D.W. Monitoring Vegetation Systems in the Great Plains with ERTS. *NASA Spec. Publ.* **1974**, *351*, 309.
40. Breiman, L. Random Forests. *Mach. Learn.* **2001**, *45*, 5–32. [CrossRef]
41. Behrouz, M.S.; Yazdi, M.N.; Sample, D.J. Using Random Forest, a Machine Learning Approach to Predict Nitrogen, Phosphorus, and Sediment Event Mean Concentrations in Urban Runoff. *J. Environ. Manag.* **2022**, *317*, 115412. [CrossRef]
42. Fang, C.; Song, C.; Wang, X.; Wang, Q.; Tao, H.; Wang, X.; Ma, Y.; Song, K. A Novel Total Phosphorus Concentration Retrieval Method Based on Two-Line Classification in Lakes and Reservoirs across China. *Sci. Total Environ.* **2024**, *906*, 167522. [CrossRef]
43. Chen, T.; Guestrin, C. XGBoost: A Scalable Tree Boosting System. In Proceedings of the 22nd ACM SIGKDD International Conference on Knowledge Discovery and Data Mining, New York, NY, USA, 13 August 2016; pp. 785–794.
44. Ramraj, S.; Uzir, N.; Sunil, R.; Banerjee, S. Experimenting XGBoost Algorithm for Prediction and Classification of Different Datasets. *Int. J. Control Theory Appl.* **2016**, *9*, 651–662.
45. Cao, Z.; Ma, R.; Duan, H.; Pahlevan, N.; Melack, J.; Shen, M.; Xue, K. A Machine Learning Approach to Estimate Chlorophyll-a from Landsat-8 Measurements in Inland Lakes. *Remote Sens. Environ.* **2020**, *248*, 111974. [CrossRef]
46. Peterson, K.T.; Sagan, V.; Sidike, P.; Hasenmueller, E.A.; Sloan, J.J.; Knouft, J.H. Machine Learning-Based Ensemble Prediction of Water-Quality Variables Using Feature-Level and Decision-Level Fusion with Proximal Remote Sensing. *Photogramm. Eng. Remote Sens.* **2019**, *85*, 269–280. [CrossRef]
47. Shang, W.; Jin, S.; He, Y.; Zhang, Y.; Li, J. Spatial–Temporal Variations of Total Nitrogen and Phosphorus in Poyang, Dongting and Taihu Lakes from Landsat-8 Data. *Water* **2021**, *13*, 1704. [CrossRef]
48. McQueen, D.J.; Lean, D.R.S.; McQueen, D.J.; Lean, D.R.S. Influence of Water Temperature and Nitrogen to Phosphorus Ratios on the Dominance of Blue-Green Algae in Lake St. George, Ontario. *Can. J. Fish. Aquat. Sci.* **1987**, *44*, 598–604. [CrossRef]
49. Lu, Y.; Li, S.; Zuo, L.; Liu, H.; Roelvink, J. Advances in Sediment Transport under Combined Action of Waves and Currents. *Int. J. Sediment. Res.* **2015**, *30*, 351–360. [CrossRef]
50. Lian, H.-S.; Liu, H.-B.; Li, X.-D.; Song, T.; Liu, S.; Lei, Q.-L.; Ren, T.-Z.; Wu, S.-X.; Li, Y. Characteristics of Nitrogen Variation and Its Response to Rainfall: A Case Study in Wuxi Port at Taihu Lake Basin. *Huan Jing Ke Xue Huanjing Kexue* **2017**, *38*, 5047–5055.
51. Sinha, E.; Michalak, A.M. Precipitation Dominates Interannual Variability of Riverine Nitrogen Loading across the Continental United States. *Environ. Sci. Technol.* **2016**, *50*, 12874–12884. [CrossRef]
52. Gallo, E.L.; Meixner, T.; Aoubid, H.; Lohse, K.A.; Brooks, P.D. Combined Impact of Catchment Size, Land Cover, and Precipitation on Streamflow and Total Dissolved Nitrogen: A Global Comparative Analysis. *Glob. Biogeochem. Cycles* **2015**, *29*, 1109–1121. [CrossRef]
53. Henson, S.A.; Cael, B.B.; Allen, S.R.; Dutkiewicz, S. Future Phytoplankton Diversity in a Changing Climate. *Nat. Commun.* **2021**, *12*, 5372. [CrossRef]
54. Winder, M.; Sommer, U. Phytoplankton Response to a Changing Climate. *Hydrobiologia* **2012**, *698*, 5–16. [CrossRef]
55. Podsetchine, V.; Schernewski, G. The Influence of Spatial Wind Inhomogeneity on Flow Patterns in a Small Lake. *Water Res.* **1999**, *33*, 3348–3356. [CrossRef]
56. Zhang, Y.; Shen, F.; Sun, X.; Tan, K. Marine Big Data-Driven Ensemble Learning for Estimating Global Phytoplankton Group Composition over Two Decades (1997–2020). *Remote Sens. Environ.* **2023**, *294*, 113596. [CrossRef]
57. Kelepertzis, E.; Argyraki, A.; Daftsis, E. Geochemical Signature of Surface Water and Stream Sediments of a Mineralized Drainage Basin at NE Chalkidiki, Greece: A Pre-Mining Survey. *J. Geochem. Explor.* **2012**, *114*, 70–81. [CrossRef]
58. Shi, K.; Zhang, Y.; Zhang, Y.; Li, N.; Qin, B.; Zhu, G.; Zhou, Y. Phenology of Phytoplankton Blooms in a Trophic Lake Observed from Long-Term MODIS Data. *Environ. Sci. Technol.* **2019**, *53*, 2324–2331. [CrossRef]
59. van Wijk, D.; Janse, J.H.; Wang, M.; Kroeze, C.; Mooij, W.M.; Janssen, A.B.G. How Nutrient Retention and TN:TP Ratios Depend on Ecosystem State in Thousands of Chinese Lakes. *Sci. Total Environ.* **2024**, *918*, 170690. [CrossRef]
60. Sinha, E.; Michalak, A.M.; Balaji, V. Eutrophication Will Increase during the 21st Century as a Result of Precipitation Changes. *Science* **2017**, *357*, 405–408. [CrossRef]

Disclaimer/Publisher's Note: The statements, opinions and data contained in all publications are solely those of the individual author(s) and contributor(s) and not of MDPI and/or the editor(s). MDPI and/or the editor(s) disclaim responsibility for any injury to people or property resulting from any ideas, methods, instructions or products referred to in the content.